Journal of Quantitative Spectroscopy & Radiative Transfer 251 (2020) 107048

Contents lists available at ScienceDirect

Journal of Quantitative Spectroscopy & Radiative Transfer

journal homepage: www.elsevier.com/locate/jqsrt

The vacuum UV photoabsorption spectroscopy of the trans-dichloroethylene (1,2-ClHC=CClH) in the 5–20 eV range: Experiment and theory

R. Locht[a,*], D. Dehareng[b], B. Leyh[a]

[a] MOLSYS Research Unit, Molecular Dynamics Laboratory, Department of Chemistry, Bldg B6c,University of Liège, Sart-Tilman, B-4000 Liège 1, Belgium
[b] Center for Protein Engineering, Department of Life Sciences, Bld-g 6a, University of Liège, Sart-Tilman, B-4000 Liège 1, Belgium

ARTICLE INFO

Article history:
Received 10 February 2020
Revised 31 March 2020
Accepted 20 April 2020
Available online 24 May 2020

Keywords:
Vacuum UV photoabsorption
Synchrotron radiation
Quantum chemical calculations
Valence and Rydberg states
Electronic and vibrational transitions
Trans-1
2-C2H2Cl2

ABSTRACT

This paper investigates in detail the vacuum UV photoabsorption spectrum of trans-1,2-$C_2H_2Cl_2$ in the 5–20 eV range using synchrotron radiation. Quantum chemical calculations are applied to the electronic transitions. Particular attention has been paid to the $2a_u(\pi)\rightarrow 2b_g(\pi^*)$ transition included in the broad band observed at 6.30 eV. The Rydberg $2a_u(\pi)\rightarrow$R3s transition is presumably observed at 6.27 eV. Below 6.0 eV the structure(s) are assigned to $\pi\rightarrow\sigma^*$ transition(s). The abundantly structured spectrum observed between 7.0 eV and 12.0 eV has been analyzed in terms of vibronic transitions to ns- ($\overline{\delta}$=0.844) and nd/4f- ($\overline{\delta}$=0.03/0.011) Rydberg states, converging to the $2a_u^{-1}$ ionization continuum, to two series of np- ($\overline{\delta}$= 0.66 and 0.40) states converging to the $5a_g^{-1}$ continuum, to ns- ($\overline{\delta}$=0.983) and nd- ($\overline{\delta}$= –0.06) states converging to the $4b_u^{-1}$ continuum and to two np-type ($\overline{\delta}$= 0.51 and 0.26) series converging to the $1b_g^{-1}$ continuum. These data are complemented by an analysis of the vibrational structure of the individual Rydberg states. Comparisons with previously reported values are provided. Several other spectral features Table S2 (see Supplementary Material) in the 12–20 eV range are tentatively assigned to transitions to Rydberg states converging to higher ionic excited states of trans-1,2-$C_2H_2Cl_2$. Assignments of the vibrational structure of some of these transitions are also proposed.

1. Introduction

Among the few spectroscopic investigations on dichloroethylenes the trans-species received the most sustained attention in the literature. To the best of our knowledge, in 1935, Mahncke and Noyes [1] were the first to photograph the vacuum UV photoabsorption spectrum (PAS) of trans-1,2-dichloroethylene between 1955 Å (6.35 eV) and 750 Å (16.53 eV). These authors presented an analysis of the bands and concluded to the absence of Rydberg transitions below 1450Å (8.55 eV). Between 65,000 cm^{-1} (8.06 eV) and 69,700 cm^{-1} (8.64 eV) a band classification was presented and a vibrational analysis was attempted.

A decade later Walsh [2] reported about a spectroscopic investigation of the five chlorine-substituted ethylenes. In the trans-1,2-isomer, Rydberg bands were classified leading to an ionization potential value of 9.91 ± 0.02 eV. A strong vibrational progression is mentioned starting at 1530 Å (8.10 eV). An analysis and assignments were proposed.

During the sixties, Goto [3] and Walsh and Warsop [4] remeasured the vacuum UV PAS of trans-dichloroethylene. The former measured the absorption coefficients in the region 2100–1050 Å (5.90–11.80 eV) and performed a superficial analysis of the spectrum. The latter authors presented an improved spectrum and focused their attention on a system of sharp bands starting at 1528 Å (8.114 eV) showing regular spacing. A detailed analysis and assignments were attempted. At short wavelengths several strong bands were localized without any further interpretation.

More recently (photo)-dissociation studies on dichloroethylenes [5-7] led to the measurement of the vacuum UV PAS of the trans-species. No original analyses or assignments were reported.

Related to vacuum UV spectroscopy, electron energy-loss spectroscopy (EELS) has been applied to chlorinated ethylenes. This technique is particularly suitable to detect singlet→triplet transitions. The energy range of 2.5-7.5 eV was investigated in six chloro-derivatives of ethylene [8]. In addition, resonance-enhanced multiphoton ionization (REMPI) spectroscopy is a very sensitive

* Corresponding author
E-mail addresses: robert.locht@ulg.ac.be, robert.locht@uliege.be (R. Locht).

https://doi.org/10.1016/j.jqsrt.2020.107048
0022-4073/

technique for the investigation of single and two-photon vibronic transitions [9] and has been applied to the dichloro-isomers of ethylene in the 65000-75000 cm^{-1} (8.06-9.30 eV) region. Detailed analyses and assignments were reported.

Only recently became *ab initio* quantum chemical calculations available on neutral states of the dichloroetylenes and more particularly on the trans-isomer [7,10]. The energy of the singlet and triplet states were calculated and compared with the available experimental results.

To complete our detailed spectroscopic study of the dichloroethylene isomers [11,12] the present work aims to describe the vacuum UV PAS of trans-1,2-dichloroethylene between 5 eV (248 nm) and 20 eV (62 nm) using synchrotron radiation. For the first time a detailed analysis of the whole energy range will be reported and assignments will be proposed based on quantum chemical calculations on the ground and excited states of the neutral and the ionized [13] molecule.

2. Experimental

2.1. Experimental setup

The experimental setup used in this work has been described previously [14]. Two monochromators were used at the BESSY synchrotron radiation facilities: (i) a modified vacuum UV normal incidence 225 McPherson monochromator with a focal length of 1.5 m (on the 1m-NIM-2 beamline at BESSY I) equipped with a gold coated laminar Zeiss grating with 1 200 lines.mm^{-1}, leading to a resolving power of 1200 at 10 eV; (ii) a 3m-NIM monochromator (on the 3 m-NIM2 beamline at BESSY II) with an Al/MgF_2 spherical grating of 600 lines.mm^{-1} reaching a resolving power of about 15000 at 10 eV (124 nm).

After the monochromator exit slit the radiation travels through a 1 mm thick stainless steel microchannel plate ensuring a differential pressure ratio of 1:1 000 with the 30 cm long stainless steel absorption cell. A Balzers capacitor manometer measures the vapor pressure in the cell and the light is detected by a sodium salicylate sensitized photomultiplier. The recording of an absorption spectrum requires one scan with gas in the absorption cell and one with the evacuated cell.

The sample pressure was kept constant at about 20 μbar to avoid saturation. Commercially available trans-1,2-$C_2H_2Cl_2$, purchased from Aldrich (98% purity) was used without further purification.

2.2. Data treatment and uncertainties evaluation

To make the identification of weak structures on a strong continuum easier, a continuum subtraction procedure has been applied. This method has already been described and used successfully in previous spectral analyses [15–18]. The underlying continuum is simulated by filtering the experimental curve by fast Fourier transform (FFT) and is then subtracted from the original photoabsorption spectrum. The resulting diagram will be called Δ-plot in the forthcoming sections.

Wavelength calibration has been performed with reference to the Ar absorption spectrum between the $^2P_{3/2}$ and the $^2P_{1/2}$ ionic states, leading to an accuracy better than 2 meV. The photoabsorption spectrum has been recorded on the 1.5m-NIM in the 6-20 eV range with an energy increment of 15 meV. The uncertainty on the energy position of a feature is estimated to be 8 meV. The photoabsorption spectra has also been recorded on the 3m-NIM between 5 eV and 15 eV with 2 meV energy steps, and in several parts of the spectrum, e.g., 8.0–9.0 eV and 11.0–12.0 eV, with 500 μeV energy steps. The uncertainty on the energy position of a feature is estimated to be less or equal to 2 meV. The reproducibility of energy positions measured in different spectra recorded over several years confirms these estimations.

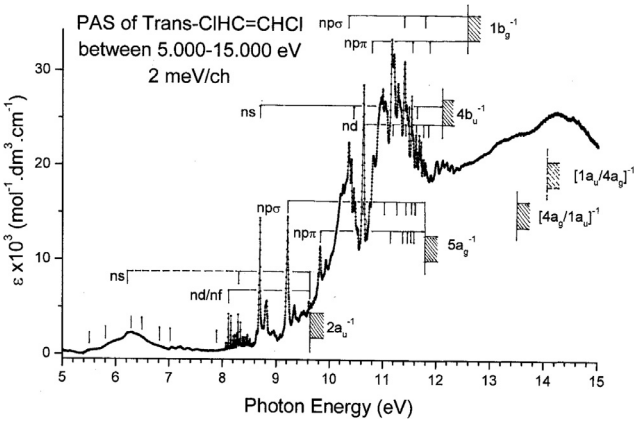

Fig. 1. VUV photoabsorption spectrum of trans-1,2-$C_2H_2Cl_2$ between 5 eV and 15, eV photon energy. Vertical bars indicate the location of valence and Rydberg transitions; shaded areas show their convergence limit [13].

Table 1
Position (eV/cm^{-1}) of maxima in the PAS band at 6.30 eV. The approximate full width half maximum (FWHM) of the peaks (meV) are inserted. Conversion factor 1 eV=8065.545 cm^{-1} [19].

Max. Continuum: 6.30 eV/50,813 cm^{-1}					
$\pi \rightarrow \pi^*(1^1B_u)$					
eV	cm^{-1}	FW HM (meV)	[1]	[4]	[5][ab]
5.18	41,800	400			
5.51	44,441	300			5.5
5.88	47,425	400			5.9
6.27	50,571	150 (3^1A_u) ($\pi \rightarrow$R3s)	6.36	6.36	6.3
6.50	52,426				6.5
6.82	55,007				6.8

[a] These values of FWHM have to be compared with 4 meV observed for Rydberg transitions.
[b] For these results: see text.

3. Experimental results

The vacuum UV PAS of trans-1,2-$C_2H_2Cl_2$ measured between 5 eV and 15 eV with energy increments of 2 meV is reproduced in Fig. 1. This spectrum can be divided into three parts: (i) between 5 eV and 8 eV and (ii) 12.0 eV and 15 eV the spectrum mainly shows only weak to very weak broad bands superimposed on a strong continuum in the latter energy range and (iii) the range between 8 eV and 12 eV displaying numerous weak to very strong and sharp features. Vertical bars indicate the energy position of the structures corresponding to valence and Rydberg transitions which will be considered in the next sections. Shaded areas indicate the different convergence limits [13]. The corresponding energy values are listed in Tables 1-3 where they are also compared to available literature data [1,2,4,9]. Owing to the large differences of their characteristics these three energy ranges will be discussed separately in the following sections.

The vacuum UV PAS recorded between 15 eV and 20 eV with 15 meV energy increments is shown in Fig. 2a. Very weak broad bands are observed and displayed in the Δ-plot shown in Fig. 2b. A curve provided by slightly smoothing the Δ-plot by fast Fourier transform (FFT) has been drawn through the noisy resulting signal. Shaded areas locate the successive ionization energies measured in

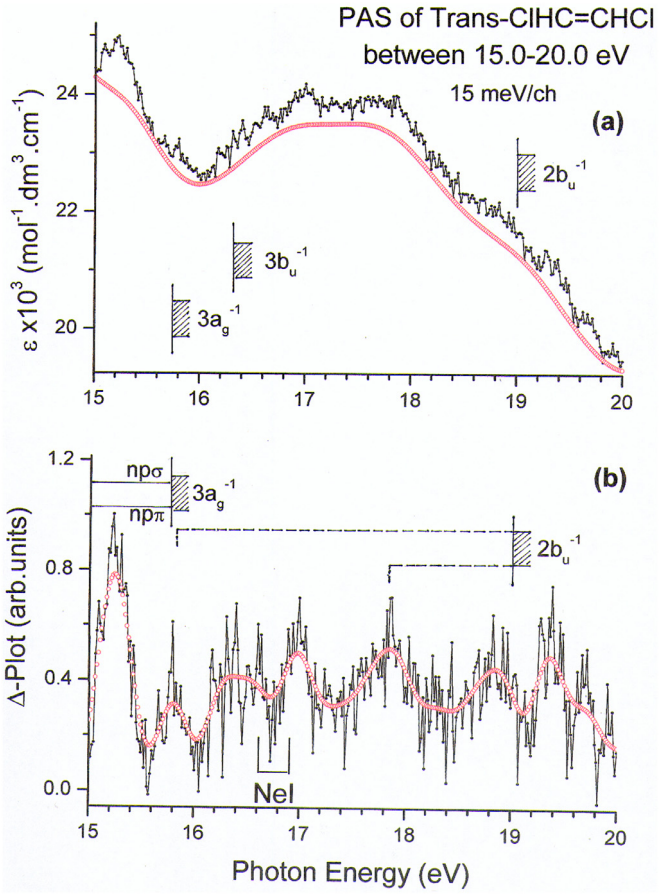

Fig. 2. VUV photoabsorption spectrum of trans-1,2-$C_2H_2Cl_2$ between 15 eV and 20 eV photon energy: (a) the direct absorbance spectrum recorded with the 1.5m NIM monochromator and 10 meV increments, (b) the Δ-plot as a function of the photon energy (eV). To the red curve correspond slightly smoothed data. Vertical bars indicate band maxima and shaded areas correspond to the ionization energies of trans-1,2-$C_2H_2Cl_2$ [13].

this photon energy range [13]. Two vertical bars indicate the NeI resonance doublet at 16.67–16.85 eV.

4. AB Initio calculations: methods and results

4.1. Computational tools

All calculations presented in this work were performed with the Gaussian 09 program [20]. The basis set used is aug-cc-pVDZ [21], containing polarization as well as diffuse functions. Some calculations were also performed without diffuse functions (basic cc-pVDZ).

The geometry optimizations have been performed at the CCSD(FC) [22,23], M06-2X [24] and TDDFT(M06-2X) [25] levels.

Wavenumbers characterizing the twelve vibrational normal coordinates were determined at the M06-2X and TDDF/M06-2X levels for the neutral ground state and the 1^1B_u excited state.

4.2. Results of the calculations

The molecular orbital configuration of trans-1,2-$C_2H_2Cl_2$ in the ground electronic state in the C_{2h} symmetry point group is described by:

$$1s(Cl1)^2, 1s(Cl2)^2, 1s(C1)^2, 1s(C2)^2, 2s(Cl1)^2, 2s(Cl2)^2,$$
$$2p_{x,y,z}(Cl1)^6, 2p_{x,y,z}(Cl2)^6$$
$$(1a_g)^2(1b_u)^2(2a_g)^2(2b_u)^2(3b_u)^2(3a_g)^2(4a_g)^2(1a_u)^2(1b_g)^2(4b_u)^2$$
$$(5a_g)^2(2a_u)^2 : \tilde{X}^1A_g$$

where $n\ell$(Cl1, Cl2, C1 and C2)^x describes the inner-shell MO by the principal (n) and angular momentum (ℓ) quantum numbers of the two Cl and C atoms. These MO are occupied by x electrons.

However, the energetic ordering of the MO's doesn't necessarily correspond to the energetic ordering of the cationic states. It agrees, however, with that considered by Von Niessen et al. [26] using the outer valence Green's function method (OVGF) and by Khvostenko [7] using the B3LYP/6-311+G(d,p) level calculations. Other calculations led to inversions of the $3a_g$-$3b_u$ [27] or the $1a_u$-$4a_g$ MO's [28] or both the $1a_u$-$4a_g$ and $3a_g$-$3b_u$ MO's [29].

The results of the geometry optimizations obtained at CCSD, M06-2X and/or TDDFT levels in the C_{2h} and C_2 symmetry point groups are presented in Table S1 (see Supplementary Material) for neutral states with a non-zero oscillator strength.

Neutral states with non-zero oscillator strength are listed in Table 4 up to 9.32 eV above the ground state. The calculated oscillator strength, excitation energy and their dominant character are indicated.

Table S2 (Supplementary Material) provides the wavenumbers of the twelve vibrational normal modes for the neutral ground and the first excited states in the C_{2h} and C_2 symmetry point groups.

At both the M06-2X and TDDFT levels the geometry optimization of the 1^1B_u state in the C_{2v} point group leads to a third order critical point (three imaginary wavenumbers; see Table S2). A true minimum could only be reached in the C_2 symmetry point group, where this state becomes 1^1B. In this configuration the $\tilde{X}^1A$ and the 1^1B states become nearly degenerate. Furthermore, this 1^1B state correlates with the excited π^* (3^1B) state of the cis-isomer [11]. It was already noticed that the cis-to-trans isomerization has to be a photo-induced process.

5. Discussion of the experimental data

In the following sections the ionization energies measured by HeI-photoelectron spectroscopy (PES) and reported recently [13] will be used. The first adiabatic ionization energy of trans-1,2-$C_2H_2Cl_2$ is $IE_{ad}(\tilde{X}^2A_u) = 9.633 \pm 0.004$ eV. The agreement with previous measurements [26–29,31,32] and accuracy have been discussed extensively [13].

The excited states of the molecular ion have also been observed and their successive adiabatic ionization energies are 11.840 eV ($\tilde{A}^2A_g$), 12.044 eV ($\tilde{B}^2B_u$), 12.582 eV ($\tilde{C}^2B_g$), 13.581 eV-14.081 eV ($\tilde{D}^2A_g$-$\tilde{E}^2A_u$), 15.725 eV-16.325 eV ($\tilde{F}^2A_g$-$\tilde{G}^2B_u$) and 19.00 eV ($\tilde{H}^2B_u$) [13,26-29].

5.1. The valence transitions between 5.0 eV and 7.0 eV (see Figs.1, 3a and 4 and Tables 1 and 4)

In the range of 5.0 eV to 7.0 eV a single broad peak is observed and displayed in Fig. 3a showing its maximum at 6.27 eV. For comparison the PAS band observed in the cis-isomer [12] is reproduced in the same figure by blue open circles. The shift of the maximum for the trans-isomer by about 300 meV to lower energies is obvious. In the literature it is usually simply assigned to the well known $\pi \rightarrow \pi^*$ transition as expected in ethylene and its derivatives (see Fig. 1 and 3a) [1,4]. Resulting from the subtraction method

Fig. 3a' clearly shows several broad features and the differences with the cis-isomer are even more apparent. Their energy position and full width at half maximum (FWHM) are listed in Table 1. Comparison is made with previous photoabsorption works [1,4].

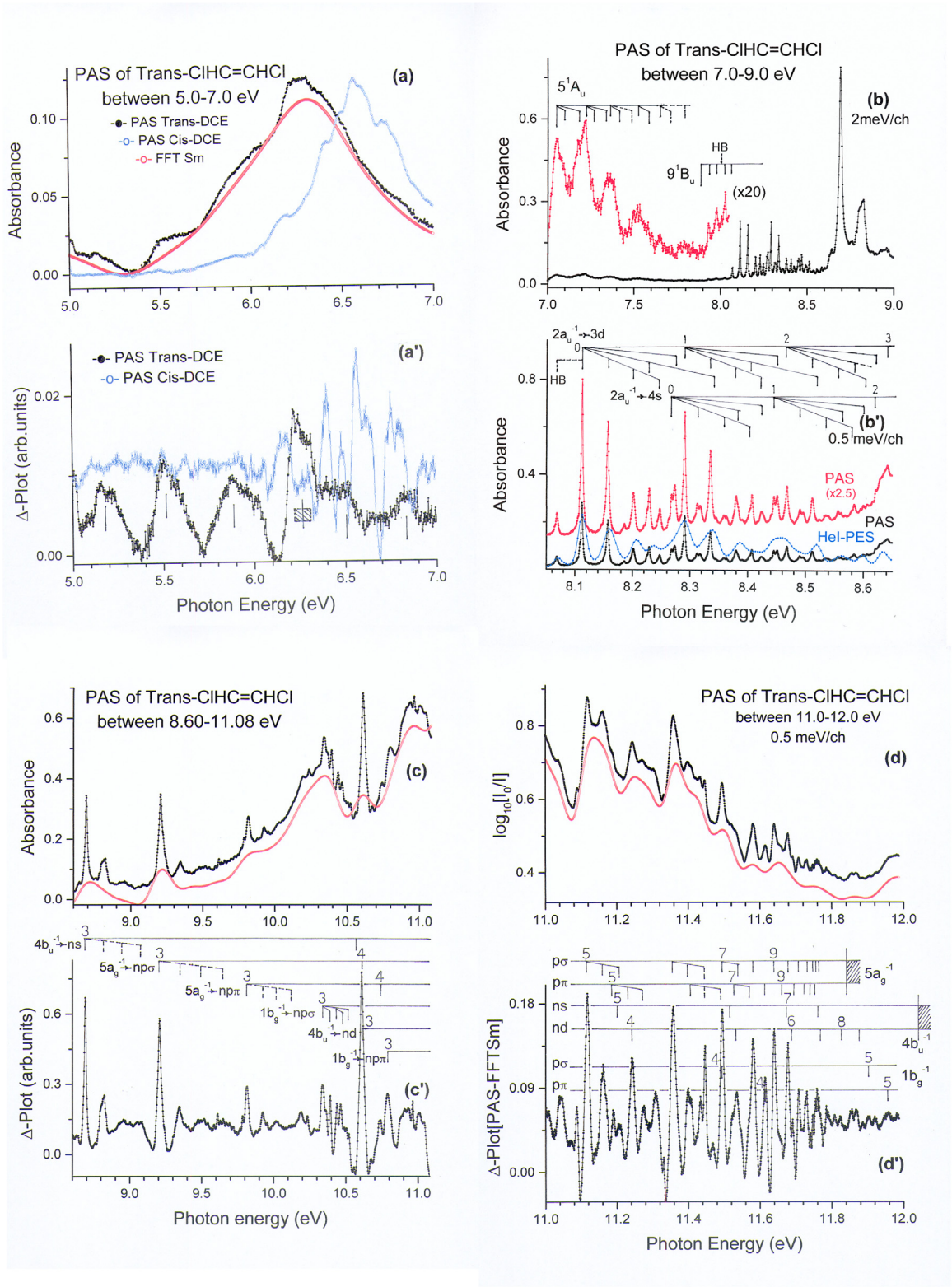

Fig. 3. VUV photoabsorption spectrum of trans-1,2-$C_2H_2Cl_2$ on an expanded photon energy scale from (a-a') 5.0-7.0 eV, (b-b') 7.0-9.0 eV, (c-c') 8.6-11.1 eV, (d-d') 11.0-12.0 eV. Vertical bars locate the strongest vibrational progressions. In (b') the blue curve corresponds to the HeI-PES band of the $\tilde{X}^2A_u$ cationic state of trans-1,2-$C_2H_2Cl_2$ [13]; the red curve corresponds to PAS amplified by the factor 2.5.

These authors mention the maximum "of a broad absorption band at 1950 Å" (6.36 eV). In the main band several more recent spectral data clearly exhibit a shoulder spreading from 5.6 eV to 6.0 eV and a long tail extending between 5.2 eV and 5.6 eV. The same features are observed in the EELS spectrum [8]. These features were not considered for discussion or assignment. The subtraction method has been applied to the digitized Fig. 7 of ref. [5]. The result is listed in Table 1.

Quantum chemical calculations presented in previous reports [7,10] and in the present work (see Table 4) agree to assign the

peak maximum at about 6.30 eV to the $2a_u^{-1}(\pi)\rightarrow 2b_g(\pi^*)$ (1^1B_u) transition with high oscillator strength. The $2a_u^{-1}(\pi)\rightarrow 3s$ (3^1A_u) Rydberg transition is calculated at 6.43 eV in this work and at 6.66 eV by Arulmozhiraja et al. [10]. This transition has very low oscillator strength. It could be assigned to the narrowest structure (150 meV) observed at 6.27 eV.

At energies below these excitations no allowed transition is calculated in the present work. However, Arulmozhiraja [10] and Khvostenko [7] located a ^1B_g state at 6.25 eV and 5.59 eV respectively and assigned it to the $2a_u^{-1}(\pi)\rightarrow 5b_u(\sigma^*)$ (^1B_g) symmetry-forbidden weak transition at 5.9 eV [5,6] and observed at 5.88 eV in the present work. Both these authors calculated lower lying $\pi\rightarrow\pi^*$ and $\pi\rightarrow\sigma^*$ transitions involving ^3B_u and ^3B_g states at 3.64 eV [7] or 3.97 [10] and 5.04 eV [7] or 6.00 eV [10] respectively.

5.2. The Rydberg transitions

The vacuum UV PAS of trans-1,2-$C_2H_2Cl_2$ (see Fig. 1) shows a very abundant structure between 8.0 eV and 14.5 eV but of very variable intensity. Most features are very sharp and superimposed on a steeply increasing continuum. Below 8.0 eV the absorption is rather weak showing very weak broad structure superimposed on a weak continuum.

In the absence of any prior information on the extent of possible Rydberg-Rydberg interactions, a first zero-order assignment of the spectral lines will be attempted, assuming the simple Rydberg formula (1) to be valid for fitting the positions in energy E_{Ryd} of the successive features:

$$E_{Ryd} = IE - R/(n-\delta)^2 = IE - R/(n*)^2 \qquad (1)$$

where R is the Rydberg constant R=13.6057 eV [19], δ is the quantum defect, n^* is the effective quantum number and IE is the convergence limit of the considered Rydberg series. These IE values have been listed earlier in this section and are inserted in Fig. 1. When the coupling between Rydberg series is negligible, the quantum defect δ has typical values which are characteristic of the angular momentum of the Rydberg orbital.

Furthermore, for centrosymmetric trans-1,2-$C_2H_2Cl_2$ belonging to the C_{2h} symmetry point group one has to apply the selection rule allowing only u↔g electronic transitions [34]. The combinations g↔g and u↔u are forbidden [34].

The fine structure observed in the spectrum will mainly be assigned to vibrational excitation associated with the successive Rydberg transitions rather than to Rydberg states particularly when high principal quantum numbers are involved. In the former case, the intensity profile follows the Franck-Condon distribution whereas in the latter the intensity is given by the n^{-3} law.

At this level we will assume that the vibrational structure involved in an electronic Rydberg transition is similar to the photoelectron band involving the ionic state to which the Rydberg series converges. This assumption implicitly also neglects perturbations due to Rydberg-Rydberg interactions. This procedure has been used successfully for the analysis of the vacuum UV spectra of C_2H_3F, 1,1-$C_2H_2F_2$ and 1,1-C_2H_2FCl [35]. To facilitate the comparison, the Δ-plot of the appropriate PAS energy range will therefore be compared to the HeI-PES of the trans-1,2-$C_2H_2Cl_2^+$ in its ground or excited states as measured in our laboratory [13].

5.2.1. Electronic Rydberg transitions

5.2.1.1. Rydberg series converging to $2a_u^{-1}$ (see Figs. 1, 3b and 4 and Table 2). The electronic Rydberg transitions associated with the first ionization limit lie between 8.11 eV and 9.63 eV. These are shown in Fig. 1 and have been listed in Table 2 together with their effective quantum numbers. In the same table the previous data reported by Mahncke and Noyes [1], Walsh [2], Walsh and Warsop [4] and Williams and Cool [9] are included for comparison. As previously mentioned (Section 2.2) the estimated error on the measurements in the present spectrum is about 2 meV or 16 cm^{-1}. Mahncke and Noyes [1] estimate the accuracy at 5 cm^{-1} for sharp bands. No error estimation is provided by the other authors [2,4,9]. To the best of our knowledge, the vacuum UV PAS of trans-1,2-$C_2H_2Cl_2$ has never been analyzed above 9.6 eV.

Table 2
Rydberg series observed in the vacuum UV photoabsorption spectrum of trans-1,2-$C_2H_2Cl_2$ converging to the adiabatic ionization energy of $\tilde{X}^2A_u$ cationic ground state at 9.633 eV [13]. Energy positions (eV), wavenumbers (cm^{-1}), effective quantum numbers n^*, quantum defects (δ) and assignments as proposed in this work. Comparison is made with the literature data [1,2,4,9]. Conversion factor 1eV= 8,065.545 cm^{-1} [19].

This Work			[1]	[2]	[4]	[9]
eV	cm^{-1}	n^*	cm^{-1}			
$2a_u^{-1}\rightarrow ndb_g$ (δ=0.03 ± 0.02)						
8.112	65,427	2.991	65,444	65,419	65,424	65,670
8.760	70,654	3.947				
$2a_u^{-1}\rightarrow ns$ (δ=0.844)						
~6.27	50,571	2.011	~51,250	~51,250	~51,216	
8.267	66,674	3.156	66,386			66,656
$2a_u^{-1}\rightarrow 4da_g$ /4f (δ=0.011)						
8.778	70,799	3.989				70,864

The first adiabatic ionization energy value $IE_{ad}(\tilde{X}\ ^2A_u)$ = 9.633±0.004 eV [13] has been used in the assignment procedure. According to electric dipole selection rules only singlet states for s- and d-type Rydberg transitions will be considered.

The first well-defined $\pi\rightarrow$ns-type Rydberg transition converging to the first ionization continuum at 9.633 eV is the $2a_u(\pi)\rightarrow 4s$ excitation observed at 8.267 eV characterized by n^* = 3.156 or δ = 0.844. Considering the n^{-3}-intensity law, the present transition would represent about 40% of the 3s transition of 0.0002 oscillator strength. In the present calculations two ^1A_u states are predicted between 8.5 eV and 8.9 eV both with very low oscillator strength. A narrow band at 66386 cm^{-1} (8.231 eV) is mentioned by Mahncke and Noyes [1] and assigned to the starting point of a vibrational progression.

As mentioned in Section 5.1 a feature is observed at about 6.27 eV shown by a dashed line in Fig. 1. This very weak feature (see also Fig. 3a) could likely be the trace of a $2a_u\rightarrow 3s$ Rydberg transition with δ=0.989. According to the present calculations this transition should have very low oscillator strength and its vertical excitation energy is predicted at 6.43 eV. Previous experimental works [1,2,4] mention a band near 51,200 cm^{-1} (6.35 eV) assigned to the usual $2a_u(\pi)\rightarrow 2b_g(\pi^*)$ transition [4].

Only the first two members n = 3 and 4 of the $2a_u(\pi)\rightarrow nd\lambda$ Rydberg series converging to the first ionization threshold are observed, with weak to very weak intensity, and an average quantum defect $\tilde{\delta}$= 0.03 ± 0.02. According to our quantum chemical calculation at the TDDFT level, the lowest allowed $\pi\rightarrow Rd_{z2}$ ($13\ ^1A_u$) transition with small oscillator strength has its vertical transition energy at 8.48 eV. This value could correspond to the adiabatic excitation energy observed at 8.112 eV being the starting point of a long vibrational progression. This value is in good agreement with all previous observations [1,2,4,9].

In the 8.75–9.15 eV energy range extremely weak and narrow features are observed superimposed on a relatively broad band with a maximum at about 8.814 eV as shown in Fig. 4a. Two recordings with 2 meV and 0.5 meV energy increments show the reproducibility of the structures. For a more detailed analysis a Δ-plot of this range has been performed and displayed in Fig. 4b. Likely vibrational progressions start at 8.760 eV and 8.779 eV for Rydberg states with quantum defects δ= 0.053 and 0.011 respectively.

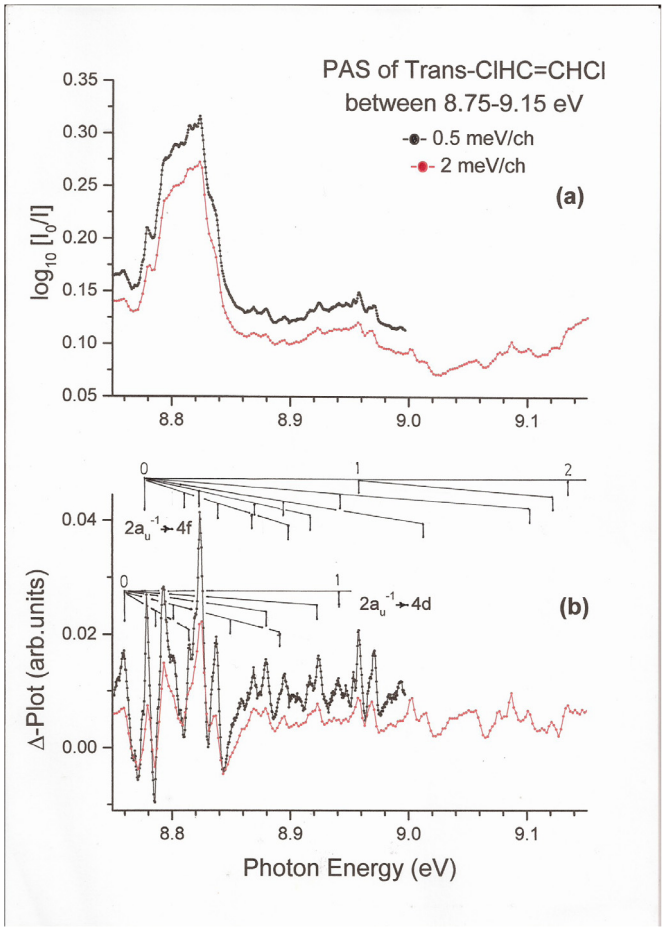

Fig. 4. (a) VUV photoabsorption spectrum of trans-1,2-$C_2H_2Cl_2$ on an expanded photon energy scale between 8.75 eV and 9.15 eV recorded with 0.5 meV (black) and 2 meV (red) increments. (b) Δ-plot of the two PAS. Vertical bars indicate the vibrational progressions.

These low δ values and the weakness of these transitions could pinpoint to (i) the $2a_u \rightarrow 4d$ Rydberg transition at 8.760 eV and (ii) the forbidden transition, e.g. a $2a_u(\pi) \rightarrow 4f$ Rydberg transition at 8.778 eV referring to Williams and Cool [9] who observed this transition at 70,864 cm^{-1} (8.786 eV). This transition is REMPI-allowed However, and keeping in mind these characteristics, a $2a_u(\pi) \rightarrow 4d\lambda$' transition could not be discarded differing from the transition measured at 8.760 eV by its angular momentum. The difference between the two adiabatic excitation energies is 0.019 eV. In the vacuum UV PAS of cis-1,2-$C_2H_2Cl_2$ transitions to nd (b_g or σ) and nd (a_g or π) Rydberg MO's are observed [12]: for n=4 the splitting is 0.029 eV. Such splitting is also observed in 1,1-$C_2H_2F_2$ and in 1,1-C_2H_2FCl where it is 0.06 eV and 0.05 eV respectively [35].

The theoretical calculations in the present work predicted a transition involving the $2a_u(\pi)$ MO with vertical excitation energy at 8.90 eV ($2a_u \rightarrow Rd_{xy}$). However, these transitions are characterized by fairly large oscillator strength.

5.2.1.2. Rydberg series converging to $5a_g^{-1}$, $4b_u^{-1}$ and $1b_g^{-1}$ (see Figs. 1 and 3b–d and Table 3). The three following ionization continua are fairly close in energy and are characterized by adiabatic transitions at 11.840 eV ($\tilde{A}^2A_g$), 12.044 eV ($\tilde{B}^2B_u$) and 12.582 eV ($\tilde{C}^2B_g$) successively [13]. Their HeI-PES [13] shows only short vibrational progressions and their adiabatic transitions dominate the spectrum. In these three ionizations mainly the non-bonding halogen MO's are involved. In the frame of our hypotheses and on the basis of these observations, an atomic-like Rydberg series spectrum is expected converging to these three ionization continua, i.e. $5a_g^{-1}$, $4b_u^{-1}$ and $1b_g^{-1}$ successively.

Considering the selection rules stated above, only $5a_g^{-1} \rightarrow np\lambda$, $nf\lambda$, ... are allowed. Table 3a lists the $5a_g^{-1} \rightarrow np$ (b_u or σ) series starting at 9.207 eV and observed for n = 3–18. An average quantum defect $\tilde{\delta}$= 0.66 ± 0.02 is obtained and only the n=16 mem-

Table 3
Rydberg series converging to the ionic excited states and observed in the vacuum UV photoabsorption spectrum of trans-1,2-$C_2H_2Cl_2$. Energy position (eV), wavenumber (cm^{-1}), effective quantum numbers (n*), average quantum defects (δ) and assignments proposed in this work. Conversion factor 1eV= 8065.545 cm^{-1} [19].

(a) Convergence to the $\tilde{A}^2$Ag at 11.840 eV (95496 cm^{-1}) [13].

eV	cm^{-1}	n*	Assign.
$5a_g^{-1} \rightarrow npb_u$ ($\bar{\delta}$= 0.66 ± 0.02)			
9.207	74,259	2.273	3
[10.605]	85,535	3.319	4
11.122	89,705	4.353	5
11.362	91,641	5.335	6
11.502	92,770	6.344	7
11.588	93,464	7.348	8
11.644	93,915	8.332	9
11.684	94,238	9.339	10
11.712	94,464	10.310	11
11.734	94,641	11.329	12
11.750	94,770	12.295	13
11.764	94,883	13.380	14
11.774	94,964	14.358	15
-	-	-	16
11.789	95,087	16.382	17
11.794	95,123	17.161	18
$5a_g^{-1} \rightarrow npa_u$ ($\bar{\delta}$= 0.40 ± 0.04)			
9.816	79,171	2.593	3
10.741	86,624	3.518	4
11.186	90,221	4.561	5
11.402	91,963	5.573	6
11.524	92,247	6.562	7
11.614	93,673	7.759	8
11.658	94,028	8.646	9
11.691	94,294	9.556	10
11.718	94,512	10.560	11
11.740	94,689	11.664	12
11.754	94,802	12.578	13
11.767	94,709	13.652	14
11.778	94,996	14.814	15
11.784	95,044	15.587	16

(b) Convergence to the $\tilde{B}^2B_u$ at 12.044 eV (97141 cm^{-1}) [13].

eV	cm^{-1}	n*	Assign.
$4b_u^{-1} \rightarrow ns$ ($\bar{\delta}$= 0.983 ± 0.005)			
8.689	70,081	2.011	3
10.559	85,164	3.018	4
11.207	90,390	4.010	5
11.513	92,859	5.019	6
11.678	94,189	6.023	7
11.777	94,988	7.021	8
$4b_u^{-1} \rightarrow nd$ ($\bar{\delta}$= −0.06 ± 0.03)			
[10.605]	85,535	3.065	3
11.242	90,673	4.095	4
11.523	92,939	5.066	5
[11.684]	[94,238]	6.072	6
[11.778]	[94,996]	6.983	7
11.836	95,464	7.918	8
11.885	95,859	9.016	9
11.919	96,133	10.076	10

(c) Convergence to the $\tilde{C}^2B_g$ at 12.582 eV (10,1481 cm^{-1}) [13].

eV	cm^{-1}	n*	Assign.
$1b_g^{-1} \rightarrow npb_u$ ($\bar{\delta}$= 0.51 ± 0.03)			
10.336	83,365	2.461	3
11.488	92,657	3.526	4
11.902	95,996	4.473	5
$1b_g^{-1} \rightarrow npa_u$ ($\bar{\delta}$= 0.26 ± 0.02)			
10.789	87,019	2.754	3
11.613	93,665	3.747	4
11.973	96,569	4.723	5

Table 4
Vertical excitation energies (eV) of neutral excited states of trans-1,2- $C_2H_2Cl_2$ computed at the TDDFT level with an aug-cc-pVDZ basis set. The main character of the involved orbitals is provided together with oscillator strengths in parentheses. Comparison is made with previous calculations at SAC-CI [10].

Neutral	E_{vert}(eV)	Description	[10]
State	TDDFT	(Oscillator Strength)	SAC-CI
1^1B_u	6.27	$\pi \rightarrow \pi^*$ (0.2815)	6.49
3^1A_u	6.43	$\pi \rightarrow Rs$ (0.0002)	6.66
5^1A_u	7.13	$\pi \rightarrow R(d+s+p)$ (0.0062)	7.44
8^1A_u	7.54	$n_{Cl}+\sigma_{CH} \rightarrow \pi^*$ (0.0006)	8.09
9^1B_u	7.68	$n_{Cl}+\sigma_{CC} \rightarrow Rp_{xy1}$ (0.0130)	8.22
13^1A_u	8.48	$\pi \rightarrow Rd_{z2}$ (0.0040)	8.30
14^1B_u	8.51	$n_{Cl}+\sigma_{CC} \rightarrow Rs$ (0.0684)	}
		$n_{Cl}+\sigma_{CH} \rightarrow Rp_{xy1}, Rp_{xy2}$	
19^1B_u	8.90	$\pi \rightarrow Rd_{zxy}$ (0.0868)	8.41
20^1B_u	8.99	$n_{Cl}+\sigma_{CC} \rightarrow Rp_{xy2}$ (0.0695)	
23^1A_u	9.16	$\pi \rightarrow Rd_{xy2}+Rs+Rd_{xy}$ (0.0297)	
24^1B_u	9.32	$\pi \rightarrow Rd_{zxy}$ (0.0261)	

ber is missing. Previous reports only mention a strong unassigned absorption band at 74,270 cm^{-1} (9.208 eV) and 85,560 cm^{-1} (10.608 eV) [1] or 74,210 cm^{-1} (9.201 eV) and 85,430 cm^{-1} (10.592 eV) [4] corresponding fairly well to the n=3 and n=4 members of the series measured in the present work at 9.207 eV (74,259 cm^{-1}) and 10.605 eV (85,535 cm^{-1}) respectively.

As shown in Table 4, quantum chemical calculations predict an energy transition to 14 ^1B_u at 8.51 eV with rather strong oscillator strength f_{osc}=0.0684. This 14 ^1B_u Rydberg state is actually characterized by a strong mixing of s- and p-type Rydberg orbitals. A theoretical prediction closer to the experimental value corresponds to a $n_{Cl}(+\sigma_{CC}) \rightarrow Rp_{xy2}$ (20 ^1B_u) transition at 8.99 eV with comparable oscillator strength f_{osc}=0.0695.

A second long Rydberg series converging to the $5a_g^{-1}$ ionization continuum starts at 9.816 eV. It is observed from n=3 up to n=16 and is characterized by an average quantum defect $\bar{\delta}$= 0.40 ± 0.04. The present value would be compatible with an npπ or npa_u Rydberg orbital. The 3pσ-3pπ/3pb_u-3pa_u splitting is 0.609 eV and is comparable to 0.586 eV measured for the same states in 1,1-$C_2H_2Cl_2$ [11].

Walsh and Warsop [4] measured a band at 79,090 cm^{-1} (9.806 eV) associated with the band at 85430 cm^{-1} (10.592 eV) and mentioned earlier in this section.

The next ionization continuum has been measured at 12.044 eV [13] and should correspond to the ionization of the non-bonding $4b_u$ (n_{Cl}) MO. The symmetry of this MO allows only electronic transitions to ns, ndλ, ... Rydberg orbitals.

The ns-Rydberg series starts at 8.689 eV and is observed up to n = 8 with an average quantum defect $\bar{\delta}$= 0.983 ± 0.005. In the literature an unassigned diffuse band is reported at 70,080 cm^{-1} (8.689 eV) [1] and 70,100 cm^{-1} (8.691 eV) [4]. Walsh [2] described the occurrence of the "strongest band of the whole spectrum" at 1427 Å (8.688 eV). This author considered this band as the n = 3 term of a series converging to 80,285 cm^{-1} (9.95 eV) with δ= –0.28. This ionization energy could not be observed in the HeI-PES [13].

Our quantum chemical calculations predict the 14 ^1B_u Rydberg state at 8.51 eV and showing a strongly mixed $n_{Cl}(+\sigma_{CC}) \rightarrow Rs$ and $n_{Cl}(+\sigma_{CH}) \rightarrow Rp_{xy}$ character with fairly strong oscillator strength (f_{osc}=0.0684). We suggest assigning the final state of the transition occurring at 8.689 eV to this 14 ^1B_u Rydberg state.

The nd-Rydberg series starts at 10.605 eV and is the strongest sharp transition observed in the spectrum. This series is observed up to n = 10 with an average quantum defect $\bar{\delta}$= –0.06 ± 0.03. This series also converges to IE_{ad}= 12.044 eV. The high intensity likely results from the superposition of at least two unresolved

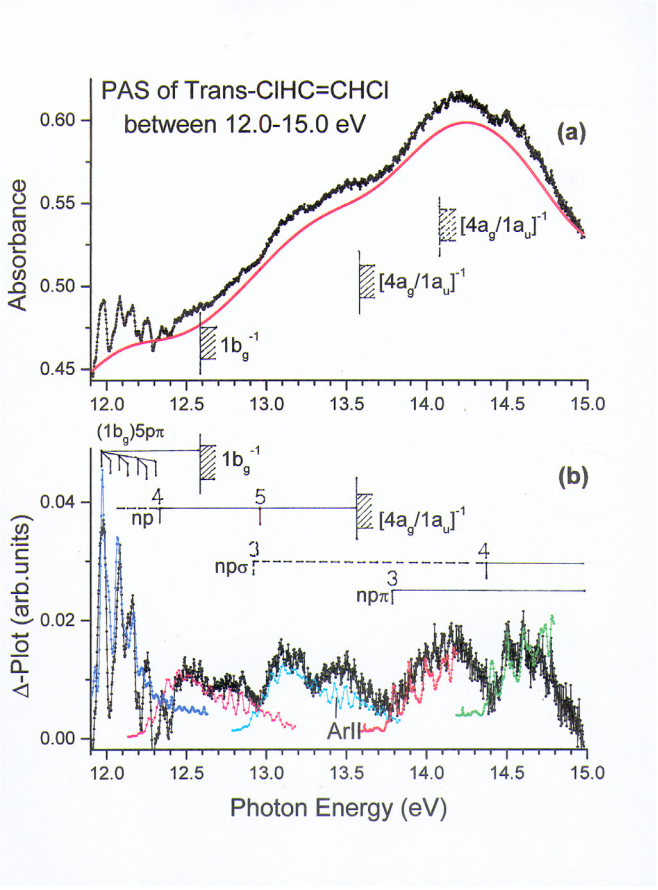

Fig. 5. VUV photoabsorption spectrum of trans-1,2-$C_2H_2Cl_2$ between 11.9 eV and 15.0 eV. Panels (a) and (b) show the absorbance and the Δ-plot respectively. Vertical bars indicate Rydberg transitions and shaded area locate the convergence limits. Colored curves correspond to HeI-PES bands [13].

contributions, i.e. the $5a_g^{-1} \rightarrow 4pb_u$ and the present $4b_u^{-1} \rightarrow 3d$ Rydberg transitions.

Pertaining to the same group of n_{Cl} MO's a last $1b_g$ orbital is predicted whose ionization has actually been measured at 12.582 eV [13]. This symmetry restricts electronic transitions to $1b_g \rightarrow np\lambda$, $nf\lambda$, ... Table 3c lists two short Rydberg series arising from transitions to $npb_u(\sigma)$ (n=3-5) starting at 10.336 eV and $npa_u(\pi)$ (n=3-5) starting at 10.789 eV. Quantum defects $\bar{\delta}$= 0.56 ± 0.06 and $\bar{\delta}$= 0.26 ± 0.02 are derived.

5.2.1.3. Rydberg states converging to $(1a_u\text{-}4a_g)^{-1}$, $(3a_g\text{-}3b_u)^{-1}$ and $2b_u^{-1}$ (see Fig. 1 and 5). In previous spectroscopic works only Mahncke and Noyes [1] mention diffuse bands at 83,761 cm^{-1} (10.385 eV) and at 87,010 cm^{-1} (10.788 eV). No analysis or assignment has been proposed by these authors. However, these bands would likely correspond to those observed at 10.336 eV and 10.789 eV in the present work.

Above 11.9 eV the vacuum UV PAS shows a short structured band between 12.0 eV and 12.3 eV followed by a slowly rising absorbance up to 15 eV. Superimposed on weak continua very weak bands with an associated vibrational structure are observed. A Δ-plot of this region is illustrated in Fig. 5b. These latter features will be analyzed in the next Section 5.2.2. Above 15 eV the spectrum only shows very weak and broad bands (see Fig. 2). Beyond 12.6 eV five ionization energies have been measured by HeI-PES [13] at 13.581 eV, 14.081 eV, 15.725 eV, 16.325 eV and 19.00 eV assigned to $1a_u^{-1}$ and $4a_g^{-1}$ ($\tilde{D}^2A_u$-$\tilde{E}^2A_g$), $3a_g^{-1}$ and $3b_u^{-1}$ ($\tilde{F}^2A_g$-G^2B_u) and $2b_u^{-1}$ ($\tilde{H}^2B_u$) ionization successively. The former four ionic states

Table 5
Energy position (eV/cm^{-1}), assignments and averaged energy / wavenumbers (Avgd.En./Wavenbr.) of the structures observed in the VUV PAS of trans-1,2-$C_2H_2Cl_2$ between 7.0 eV and 8.0 eV. Comparison is made with earlier data [1,2,4]. Conversion factor 1eV= 8065.545 cm^{-1}[19].

(a)

eV	cm^{-1}	Assign.	[9]	Avgd.En./Wavenbr.
7.051	56,870	(0,0,0)		**5^1A_u**
7.093	57,209	ν_5		
7.172	57,846	ν_4		ω=0.168 ± 0.002 eV
7.215	58,193	$\boldsymbol{\nu}$		1,355 ± 16 cm^{-1}
7.257	58,532	$\nu+\nu_5$		(ωx=0.003 ± 0.001 eV
7.341	59,209	$\nu+\nu_4$		24 ± 8 cm^{-1})
7.369	59,435	$\boldsymbol{2\nu}$		ω_4=0.126 ± 0.007 eV
7.405	59,725	$2\nu+\nu_5$	59,656	1,016 ± 60 cm^{-1}
7.502	60,508	$2\nu+\nu_4$	60,587	ω_5=0.043 ± 0.007 eV
7.524	60,685	$\boldsymbol{3\nu}$		347 ± 60 cm^{-1}
7.579	61,129	$3\nu+\nu_5$	61,114	
7.656	61,750	$\boldsymbol{4\nu}$	61,700	
7.690	62,024	$4\nu+\nu_5$	62,009	
7.790	62,831	$\boldsymbol{5\nu}$	62,880	

(b)

eV	cm^{-1}	[4]	[9]	Assign.	Avgd.En./Wavenbr.
7.884	63,589	-	63,571	(0,0)	**9^1B_u (7^1B_g, 11^1A_g)**
7.930	63,960	63,961	63,924	ν_5	ω_5=0.044 ± 0.003 eV
7.978	64,347	64,304	64,272	$2\nu_5$	355 ± 20 cm^{-1}
8.020	64,686	64,572	64,647	$3\nu_5$	
8.026	64,734	64,724	64,799	HB/R	
8.052	64,944	-		na	
8.060	65,008	-		$4\nu_5$	

HB/R: hot band of Rydberg state at 8.112 eV.

overlap two by two in the HeI-PES [13]. It has to be reminded (see Section 4.2) that the ordering of the $1a_u$ and $4a_g$ MO's adopted in the present work appears inverted in some previous PES and theoretical works [28,29]. This is also the case of the $3a_g$-$3b_u$ sequence [27,29]. The ordering of the orbitals will be tested on the basis of already stated selection rules.

A fairly well isolated structured band starts at 11.973 eV. It is assigned to the $5pa_u$ member of the Rydberg series converging to the $1b_g{}^{-1}$ ionization continuum. The excitations occurring above 12.3 eV have most likely to be assigned to transitions to Rydberg states of series converging to 13.581 eV-14.081 eV and 15.725 eV-16.325 eV. Close to and above 19.0 eV the Rydberg bands should converge to ionized states above 20 eV, e.g. at 22.4 eV [26,28].

As will be discussed in Section 5.2.2, beyond 12.4 eV and up to 14.8 eV an abundant long fine structure is observed uninterruptedly with a slightly modulated intensity. The HeI-PES bands measured at 13.581 eV and 15.725 eV are abundantly structured [13] both with a well-defined adiabatic ionization energy.

Despite the difficulty to define precise excitation energies, two weak absorption bands seem to start at about 12.35 eV and 12.96 eV successively. The shape of the bands is close to that of the $\tilde{D}^2A_u$-$\tilde{E}^2A_g$ HeI-PES band [13] as is illustrated in Fig. 5b. The derived effective quantum numbers n*=3.32 and 4.52 provide quantum defects δ=0.68 and 0.48. These values are typical for np-type Rydberg states. Based on the selection rules, transitions to np-Rydberg states imply a g-type starting orbital, i.e. the a_g MO available at this energy. Therefore, it would be very likely that the actual energetic ordering would be $4a_g$-$1a_u$ instead of $1a_u$-$4a_g$ as found out by the present calculations where the corresponding ionic states are nearly degenerate at the TDDFT level [see Table 3 in ref. 13]. However, this finding would agree with the orbital ordering proposed by Brendtsson et al. [28] and Mei et al. [29].

Slightly more obvious are the two bands starting at about 13.8 eV and 14.4 eV. Their profile is close to that of the $\tilde{F}^2A_g$-band in the HeI-PES [13] with IE_{ad} = 15.725 eV as illustrated in Fig. 5b. Taking this ionization limit, n* = 2.65 (δ = 0.35), and n* = 3.217 (δ = 0.78) are derived at 13.80 eV and 14.40 eV respectively. These values of the quantum defect could point to transitions to $3pa_u(\pi)$ and to $4pb_u(\sigma)$ Rydberg states. Under the selection rules stated above the $3a_g$ orbital should be involved at 15.725 eV followed by the $3b_u$ orbital. This finding is in agreement with the energetic ordering predicted in the present work. A reversed sequence has been proposed in the literature [27,29].

As shown in Fig. 2 the 15–20 eV range consists of a few very weak broad bands. Above the $3a_g$-$3b_u$ doublet PES band the last ionic state below 21.22 eV is observed at 19.00 eV. HeII-PES [26], Al-Kα-PES [28] and EELS [29] reveal inner-valence shell ionization at 22.4 eV, 25.6 eV and 27.1 eV successively. The broad bands at about 15.8 eV and 17.8 eV could likely be assigned to 3s- and 3d-Rydberg states converging to the ionization threshold at 19.0 eV.

5.2.2. Vibrational valence/Rydberg transitions

Several electronic transitions observed in the present vacuum UV PAS show extended vibrational structure. On the basis of the hypotheses stated above, an analysis of this structure will be attempted in the following sections.

5.2.2.1. Valence/Rydberg states in the 7–8 eV range (see Figs. 3b and 6 and Table 5). In this photon energy range two weak and very weak transitions are observed at 7.051 eV and 7.884 eV successively. Between 7.051 eV and 7.790 eV the bands are broad and structured with various shapes. In the narrow range of 7.884 eV and 8.060 eV the bands look as much sharper single peaks. Only Walsh and Warsop [4] reported bands between 63,961 cm^{-1} (7.930 eV) and 64,724 cm^{-1} (8.025 eV) without analysis or assignment. The energy position of the structures as measured in the present work is listed in Tables 5a and 5b.

The lowest ionization continuum is measured at 9.633 eV [13] involving the $2a_u$ MO. In account of the selection rules only

Table 6
Energy position (eV/cm^{-1}), assignments and averaged energy / wavenumbers (Avgd.En./Wavenbr.) of the structures observed in the VUV PAS of trans-1,2-$C_2H_2Cl_2$ between 8.02 eV and 8.64 eV.Comparison is made with earlier data [1,2,4,9]. Conversion factor 1eV= 8,065.545 cm^{-1}[19].

Rydb.Trans. $[2a_u(\pi)]^{-1}\rightarrow 3d$; δ=0.009						
eV	cm^{-1}	[1]	[2]	[4,9][a]	Assign.	Avgd.En./.Wavenbr.
8.026	64,734			64,724	HB	**$\pi\rightarrow$3d Rydberg**
8.052	64,944				na	ω_1=0.395 ± 0.001 eV
8.069	65,089	65,096		65,076	HB	3186 ± 8 cm^{-1}
8.097	65,307				na	ω_2=0.180 ± 0.001 eV
8.105	65,371				na	1452 ± 8 cm^{-1}
8.109	65,403				*	($\omega_e x_e$=0.0013 ± 0.0003 eV
8.112	65,428	65,444	65,419	65,424	**3d(0,0)**	10.5 ± 2.4 cm^{-1})
8.121	65,500				na	ω_3=0.161 ± 0.001 eV
8.128	65,557				na	1298 ± 8 cm^{-1}
8.141	65,662			[65670]	[ν_{12}]	ω_4=0.117 ± 0.003 eV
8.146	65,702			[65688]	na	944 ± 24 cm^{-1}
8.152	65,750				*	ω_5=0.044 ± 0.001 eV
8.157	65,791	65,813	65,789	65,787	ν_5	355 ± 8 cm^{-1}
8.169	65,887				[$2\nu_{12}$]	[ω_{12}=0.029 ± 0.001 eV
8.175	65,936				na	234 ± 8 cm^{-1}]
8.186	66,025	66,032		[66031]	[$\nu_5+\nu_{12}$]	
8.197	66,113			[66060]	[$3\nu_{12}$]	
8.201	66,146	66,174	66,151	66,154	$2\nu_5$	
8.211	66,226				[$\nu_5+2\nu_{12}$]	
8.217	66,274				na	
8.220	66,299				na	
8.225	66,339		66,335	[66359]	[$4\nu_{12}$]	
8.229	66,371			66365	[$2\nu_5+\nu_{12}$]	
8.231	66,387	66,386			ν_4	
8.242	66,476			[66450]	[$\nu_5+3\nu_{12}$]	
8.244	66,492				*	
8.247	66,517			66,523	$3\nu_5$	
8.250	66,541	66,541			na	
8.258	66,605				[$\nu_4+\nu_{12}$]/ [$2\nu_5+2\nu_{12}$]	
8.263	66,646			[66,656]		
8.273	66,726			66,716	ν_3	
8.276	66,750	66,752		[66727]	$\nu_4+\nu_5$	
8.283	66,807			[66748]	na	
8.287	66,839			[66823]	[$\nu_4+2\nu_{12}$]/ [$2\nu_5+3\nu_{12}$]	
8.291	66,871	66,891	66,863	66872	ν_2	
8.307	67,000			[67032]	na	
8.317	67,081			67071	[$\nu_4+3\nu_{12}$]/ [$2\nu_5+4\nu_{12}$]	
8.320	67,105	67,111		[67103]	[$\nu_2+\nu_{12}$]	
8.330	67,186			[67123]	$\nu_4+2\nu_5$	
8.335	67,226	67,263	67,222	67,234	$\nu_2+\nu_5$	
8.344	67,299				$2\nu_4$	
8.356	67,396				na	
8.363	67,452	67,466		67,433	na	
8.375	67,549				$\nu_4+3\nu_5$	
8.380	67,589	67,621	67,590	67,601	$\nu_2+2\nu_5$	
8.407	67,807	67,835	67,770	67,801	$\nu_2+\nu_4$	
8.417	67,888				$\nu_2+3\nu_5$	
8.424	67,944	67,954		67,958	na	
8.446	68,121	68,137		68,141	$2\nu_3$	
8.451	68,162	68,188			$\nu_2+\nu_3$	
8.468	68,299	68,322	68,292	68,297	$2\nu_2$	
8.507	68,614			68,491	ν_1	
8.511	68,646	68,676	68,655	68,657	$2\nu_2+\nu_5$	
8.524	68,751				$\nu_2+2\nu_4$	
8.556	69,009	68,892	69,056	69,034	$2\nu_2+2\nu_5$	
8.568	69,106				na	
8.584	69,235	69,249	69,223	69,215	$2\nu_2+\nu_4$	
8.595	69,324				$2\nu_2+3\nu_5$	
8.600	69,364					
8.616	69,493				$\nu_2+2\nu_3$	
8.629	69,598				$2\nu_2+\nu_3$	
8.634	69,638				na	
8.637	69,662				na	
8.639	69,678				na	
8.641	69,694	69,701		69,700	$3\nu_2$	

HB: hot band; na: not assigned; *: discussed in text.
[a] Data in brackets in this column are from ref. [9].

Table 7
Valence and first Rydberg transition energies (eV) measured in the three dichloroethylene isomers; (v) indicates the presence of vibrational structure.

Transit.	1,1-[11]	Cis-1,2[12]	Trans-1,2
$\pi\rightarrow\pi^*$	6.15(v)	6.16(v)	6.30
$\pi\rightarrow\sigma^*$	5.1(v) and below	5.1(v) and below	5.9 and below
$\pi\rightarrow$R3s	6.75(v)	6.40(v)	6.27

transitions to ns and ndλ Rydberg orbitals would be allowed. Alternatively, considering the weakness of these transitions, particularly at 7.884 eV and beyond, the forbiddance could be invoked on e.g. a transition to a 3p Rydberg orbital. Such a transition has been observed by REMPI as a strong two-photon transition between 59,656 cm^{-1} and 64,799 cm^{-1} [9].

The present quantum chemical calculations predict the existence of several neutral states in this energy range. Close to 7.0 eV the 5^1A_u, 8^1A_u and the 9^1B_u states have been calculated. They have non-zero but weak oscillator strength. The 5^1A_u has a (d+s+p)-Rydberg character whereas the 9^1B_u state has a better defined Rydberg-p character and these states carry weak oscillator strengths. The 8^1A_u is a ($n_{Cl}+\sigma_{CH}$)-type valence state and the corresponding transition is predicted to be of very weak oscillator strength. Beside these allowed transitions several forbidden states are calculated: 4^1B_g (at 6.90 eV), 6^1B_g (7.21 eV) and 7^1B_g (7.52 eV). The 4^1B_g and 7^1B_g show pure Rydberg (Rp_{xy})-character whereas the 6^1B_g is of ($n_{Cl}+\sigma_{CC}$) valence-type. However, it has to be noticed that in their paper Arulmozhiraja et al. [10] reported a 2^1A_u state at 7.44 eV (corresponding to the present 5^1A_u) assigning it to a mixed π-3dσ/π-σ^* Rydberg-valence character. Their 3^1A_u at 8.09 eV (corresponding to the present 8^1A_u) also has a mixed Rydberg-valence n-π^*/π-3dσ character.

Using the peak shape as additional information, we suggest that the transitions starting at 7.051 eV would be valence-valence with weak oscillator strength. As shown in Table 4 the 5^1A_u state calculated at 7.13 eV is a suitable candidate. The detailed vibrational structure is shown in Fig. 3b. The corresponding positions are listed in Table 5a and the excitation energies $EE_v(v)$ and $\Delta G_v(v)$-plots are displayed in Fig. 6. These diagrams lead to a vibrational wavenumber of ω=1,355 ± 16 cm^{-1} (0.168 ± 0.002 eV) and an anharmonicity constant ωx = 24 ± 8 cm^{-1} (0.003±0.001 eV). The value of the wavenumber lying between ω_2^+=1,452 cm^{-1} (C=C stretch) and ω_3^+=1,258 cm^{-1} (C-H bending) measured for the cation [31,32] prevents any unambiguous assignment. Combined with this vibration two other wavenumbers are measured: 1,016 ± 60 cm^{-1} (0.126 ± 0.007 eV) and 347 ± 60 cm^{-1} (0.043 ± 0.007 eV). Both wavenumbers are fairly close to the corresponding values measured by other techniques for the ground state cation, i.e. ω_4^+=944 cm^{-1} (C-Cl stretching) and ω_5^+=365 cm^{-1} (mainly C=C-Cl bending) [31,32].

A very weak and short progression starts at 7.884 eV showing narrow peaks possibly for dominant Rydberg character and assigned to 9^1B_u. Its structure clearly shows only one wavenumber ω_5=355 ± 20 cm^{-1} (0.044 ± 0.003 eV). This single value is close to ω_5^+=365 cm^{-1} [31,32] observed for the cation. Using EE_{ad}^{Ryd}=7.884 eV and IE_{ad}=9.633 eV a value n^*=2.789 and a quantum defect δ=0.211 are obtained and could possibly correspond to a $2a_u\rightarrow$3p(σ or b_u) transition. Such transitions have been calculated for the 7^1B_g state at 7.52 eV and the 11^1A_g state at 7.87 eV in the present work and at 7.72 eV for the 3^1B_g state by Arulmozhiraja et al. [10] but have zero oscillator strength. Transitions to all these states are not allowed. As mentioned in Table 5b the present measurements agree with those reported by Walsh and Warsop [4]. Most of them also correlate well with REMPI data assigned to $2a_u\rightarrow$3p transitions [9].

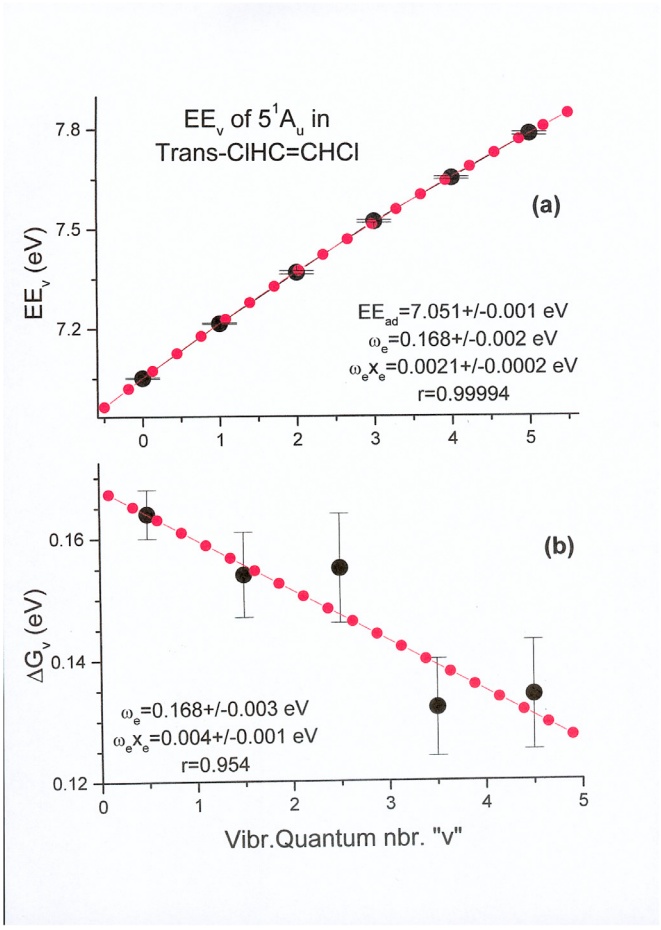

Fig. 6. Excitation energy EE_v (a) and ΔG_v (b) plots as a function of the vibrational quantum number v for the 5^1A_u state. The values of the parameters are included.

5.2.2.2. Rydberg states converging to $2a_u^{-1}$ (see Figs. 1,3b and Tables 6 and S3). Between 8.026 eV and 8.652 eV the vacuum UV PAS of trans-1,2-$C_2H_2Cl_2$ shows a very abundant but weak structure with sharp features. Several of them appear with multiple components. The HeI-PES of the $\tilde{X}$ X^2A_u state of the cation [13] inserted in Fig. 3b' (blue curve) reproduces roughly the vacuum UV PAS and helps to locate the strongest features in the PAS. The proposed assignments are inserted in Fig. 3b', listed in Table 6 and are also compared to those reported in previous works [1,2,4,9].

Very weak signals are detected below 8.112 eV and have been assigned to hot bands (HB). The intensity of the transitions at 8.026 eV and 8.069 eV represent respectively 3.5% and 20% of the adiabatic transition intensity measured at 8.112 eV. In agreement with the Maxwell-Boltzman distribution-law these features have to be assigned to transitions from v=2 and 1 of the ν_5 mode (C=C-Cl bending of 330 cm^{-1} [33]).

Up from 8.112 eV the strongest progression shows an averaged ϖ_2=1,452±8 cm^{-1} (0.180±0.001 eV) and is observed up to v=3. In combination with this progression three other wavenumbers are unambiguously detected, i.e. ω_3=1,298 ± 8 cm^{-1} (0.161 ± 0.001 eV), ω_4=944 ± 24 cm^{-1} (0.117 ± 0.003 eV) and ω_5=355 ± 8 cm^{-1} (0.044 ± 0.001 eV). The weakest but still significant signal is easily observed between the major peaks at regular intervals of about 29 meV. The average is ϖ=234 ± 8 cm^{-1} (0.029 ± 0.001 eV). It frequently appears in combination with ν_4 and ν_5 and is observed between 8.112 eV and 8.320 eV. The steep

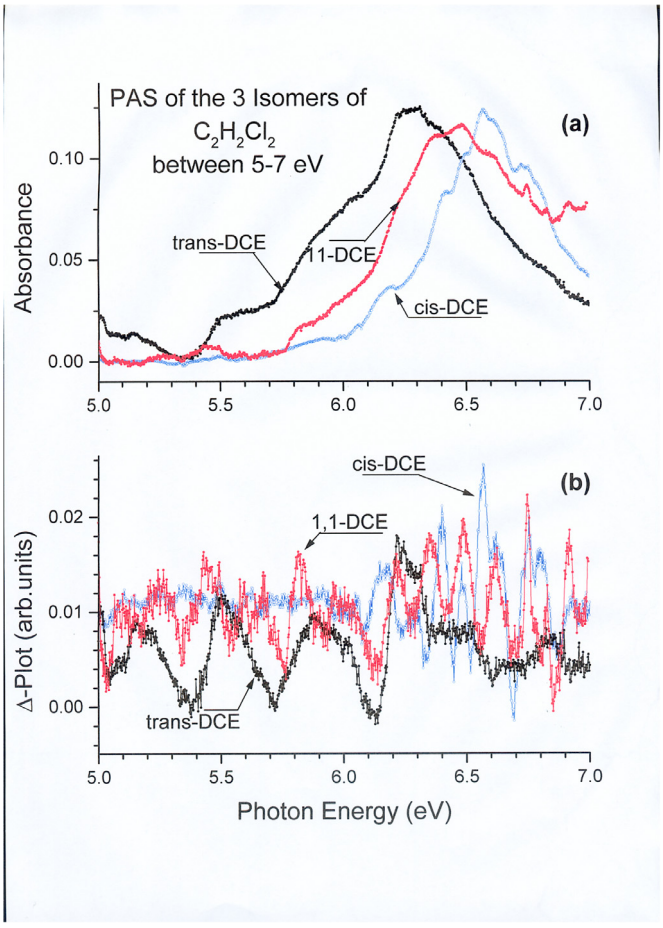

Fig. 7. Comparison of the 5.0-7.0 eV band in the VUV photoabsorption spectrum of the three dichloroethylene isomers in (a) the original spectrum and (b) the corresponding Δ-plots (black trans-1,2; blue cis-1,2; red 1,1-isomer).

intensity decrease of the absorption would likely prevent to observe this vibration at higher energy. This low wavenumber best corresponds to ν_{12} of b_u symmetry (anti-symmetric H-C-Cl bending) but is symmetry forbidden (in agreement with the very weak intensity observed). The corresponding wavenumber in the ground state of the cation is $\omega_{12}{}^{+}$=251 cm^{-1} [32] and in the neutral ground state ω_{12}=250 cm^{-1} [33].

A last very weak transition is observed at 8.507 eV which has tentatively been assigned to ω_1=3,186 ± 8 cm^{-1} (0.395 ± 0.001 eV) corresponding to C-H stretching. This vibration was not observed previously by optical spectroscopy [1,2,4] or by electron spectroscopy [31,32]. In the neutral $\tilde{X}^1A_g$ ground state ω_1=3,073 cm^{-1} [33], whereas in the $\tilde{X}^2A_u$ cationic ground state $\omega_1{}^{+}$=3,121 cm^{-1} [31].

As already mentioned numerous bands show up as multiplets but are weaker than the $2a_u \rightarrow 3d$ Rydberg transition. The transition measured at 8.267 eV should correspond to the $2a_u \rightarrow 4s$ Rydberg transition with n*=3.156 and δ=0.844. The analysis of this electronic transition provides four wavenumbers: ω_2=1,428 ± 24 cm^{-1} (0.177 ± 0.003 eV), ω_3=1,290 cm^{-1} (0.160 eV), ω_4=928 ± 60 cm^{-1} (0.115 ± 0.008 eV) and ω_5=355 ± 30 cm^{-1} (0.044 ± 0.004 eV) (see Table S3a). All these figures are close to those measured for the $2a_u \rightarrow 3d$ transition.

Between 8.760 eV and 9.135 a very weak but sharp series of structure has been highlighted (see Fig. 4a) superimposed on a weak broad band. The reproducibility of the details of this sequence has been tested by recording this region with different definitions, i.e. 2 meV and 0.5 meV energy increments. Fig. 4b shows the corresponding Δ-plots and the result of the analysis of this structure is listed in Table S3b.

Two very weak Rydberg transitions might be involved, i.e. $2a_u \rightarrow 4d$ at 8.760 eV and $2a_u \rightarrow 4f$ at 8.779 eV. The corresponding quantum defect is δ=0.053 and 0.011 respectively. The energy position of the successive features and their assignment are listed in Table S3b. For the 4d-Rydberg state ω_2=1,419 cm^{-1}, ω_3=1,323 cm^{-1}, ω_4=960 cm^{-1} and ω_5=347 ± 24 cm^{-1}. For the 4f-Rydberg state ω_2=1,452 ± 16 cm^{-1}, ω_3=1,290 ± 16 cm^{-1}, ω_4=944 ± 40 cm^{-1} and ω_5=355 ± 8 cm^{-1}. For both the 4d- and 4f-Rydberg states the forbidden ν_{12} vibration is also likely involved with $(\omega_{12})_{4d}$=242 ± 24 cm^{-1} and $(\omega_{12})_{4f}$=234 ± 8 cm^{-1}. All these results are very close to those provided by previous analyses of the Rydberg states converging to the $2a_u{}^{-1}$ ionization continuum. Even if the 4f transition is symmetry forbidden, the major arguments for this assignment are (i) its weakness and (ii) the fairly good correlation of many positions determined in the present work and those reported in the REMPI work of Williams and Cool (see Table XII in ref. [9]).

5.2.2.3. Rydberg series converging to $5a_g{}^{-1}$, $4b_u{}^{-1}$ and $1b_g{}^{-1}$ (see Figs. 3c-d and 5). These Rydberg transitions mainly cover the 8.6-12.6 eV photon energy range. This region includes the strongest bands observed in the PAS involving $4b_u{}^{-1} \rightarrow 3s$, $5a_g{}^{-1} \rightarrow 3pb_u(\sigma)$ and $5a_g{}^{-1} \rightarrow 3pa_u(\pi)$ transitions and all are followed by weak to very weak structures. Similarities in the spectra are indicated in Fig. 3c by dashed lines pointing out the position of maxima and likely providing two wavenumbers, i.e. about 860 cm^{-1} and 1,170 cm^{-1}. Clearly a short wavenumber of about 320 ± 30 cm^{-1} (0.040 ± 0.004 eV) is present and superimposed on these maxima, particularly well observed between 9.4 eV and 9.8 eV. This latter wavenumber is usually linked to ν_5 (C=C-Cl bending) vibration.

The two transitions at 10.336 eV (see Fig. 3c) and at 11.973 eV (see Fig. 5) show better defined structures linked to the $\tilde{C}^2B_g$ cationic state [13]. The $3pb_u(\sigma)$ state shows ω_4=740 ± 30 cm^{-1} and ω_5= 454 ± 30 cm^{-1} probably linked to $\omega_4{}^{+}$=840cm^{-1} and $\omega_5{}^{+}$= 340 cm^{-1} measured for the cation [13]. The $5pa_u$ Rydberg band is well fitted by the $\tilde{C}^2B_g$ HeI-PES band as shown in Fig. 5: ω_4=920 ± 30 cm^{-1} and ω_5= 322 ± 60 cm^{-1} are estimated and have to be compared with $\omega_4{}^{+}$=840 cm^{-1} and $\omega_5{}^{+}$= 340 cm^{-1} respectively, as measured for the $\tilde{C}^2B_g$ cation [13].

5.2.2.4. Rydberg series converging to $(4a_g\text{-}\ 1a_u)^{-1}$ and $(3a_g\text{-}3b_u)^{-1}$ (see Fig. 5). As discussed in Section 5.2.1.3 the actual MO sequence is likely $4a_g$ followed by $1a_u$ upon increasing energy. The corresponding ionizations give rise to two overlapping HeI-PES bands [13]. These are reproduced in Fig. 5b. Despite the low signal/noise ratio a very weak but detectable vibrational progression is observed between 12.4 eV and 13.6 eV. In the attempt to disentangle this structure the HeI-PES is used and its profile reproduces fairly well the PAS band (see Fig. 5b). Starting at 12.345 eV and up to 12.91 eV two wavenumbers account for the observed features: ω_A=766 ± 20 cm^{-1} (0.095 ± 0.003 eV) and ω_B=298 ± 20 cm^{-1} (0.037 ± 0.003 eV). Between 12.96 eV and 13.64 eV a similar progression is observed with ω_A'=742 ± 40 cm^{-1} (0.092 ± 0.005 eV) and ω_B'=314 ± 60 cm^{-1} (0.039 ± 0.007 eV). These figures can be compared to those measured in the $\tilde{D}$-$\tilde{E}$ cationic states where the C=C-H bending (ν_4) and the H-C-Cl bending (ν_5) vibrations would be involved respectively [13].

From 13.8 eV and up to 14.8 eV two well separated broad bands are observed. Both are made of vibrational progressions clearly emerging from the noise. As shown in Fig. 5, between 13.8 eV and 14.2 eV the HeI-PES band profile reproduces fairly well the PAS band shape. However, the HeI-PES band of the $\tilde{F}^2A_g$ state shows intensity alternation [13] not observed in the corresponding PAS band (13.8-14.8 eV). This leads to three alternative assign-

ments: this band is made of (i) a unique progression with ω= 411 ± 60 cm^{-1} (0.051 ± 0.007 eV) or (ii) a progression consisting of two wavenumbers ω_A=839 ± 50 cm^{-1} (0.104 ± 0.006 eV) and ω_B=411 ± 70 cm^{-1} (0.051 ± 0.008 eV) and finally (iii) two overlapping bands each with a progression characterized by $\omega\approx$840 cm^{-1}. Though a definite assignment is difficult, it has to be stressed that the alternative (ii) is consistent with the assignment made for the $\widetilde{F}^2A_g$ ionic state where ω_A and ω_B correspond to ν_4^+(C=C-H bending) and ν_5^+(H-C-Cl bending) respectively with wavenumbers measured at 847 cm^{-1} and 363 cm^{-1} [13]. The second band starting at 14.434 eV is well fitted by the $\widetilde{F}^2A_g$ HeI-PES band as shown in Fig. 5. The wavenumber measured in this case is ω_4= 758 ± 20 cm^{-1} (0.094 ± 0.003 eV). Clearly a smaller wavenumber is present but difficult to measure owing to the unfavorable signal/noise ratio. Though smaller, this wavenumber might be assigned to ν_4 (C=C-H bending) vibrational motion.

6. Conclusion

The vacuum UV PAS of trans-1,2-$C_2H_2Cl_2$ presented in this work is obtained by using synchrotron radiation. It is investigated between 5 eV and 20 eV for the first time. Quantum chemical calculations were performed to help assigning the transitions observed in the spectrum. The associated oscillator strengths are eValuated. Particular attention has been paid to the dynamics of the 1^1B_u state involved in the $\pi\rightarrow\pi^*$ transition.

At low energy, i.e. between 5 eV and 7 eV the usual broad band actually consists of several broad structures of low intensity which may likely be assigned to $\pi\rightarrow\sigma^*$ (below 6.0 eV), $\pi\rightarrow\pi^*$ (at 6.30 eV) and $\pi\rightarrow$3sR (at 6.27 eV).

At intermediate energy, i.e. from 8 eV to 15 eV, a few very strong and many weak to very weak Rydberg transitions are observed and interpreted. Several of the Rydberg states involved show an extensive vibrational structure. Vibrational wavenumbers and assignments are proposed.

In the range of 15 eV to 20 eV photon energy only very weak broad and apparently structureless bands are observed and assigned to Rydberg transitions converging to the outer-valence shell ionization $2b_1^{-1}$ (at 19.0 eV) and to inner-valence shell ionization $1b_u^{-1}/1a_g^{-1}$ (at 22.4 eV [26,28]).

The present work completes the detailed study of the vacuum UV PAS of the three dichloroethylene isomers [11,12] in the 5 eV to 20 eV photon energy range. The most obvious but unexpected observation is the large difference in shape of the vacuum UV-PAS of the three isomers. However, the three spectra are very similarly dominated by the very strong $n_{Cl}\rightarrow$Rydberg MO transitions. Except for the 1,1-isomer these show short vibrational progressions. On the contrary the Rydberg transitions starting from the π(C=C) MO are weak to very weak in the three spectra and exhibit extended vibrational progressions.

Owing to its importance in photochemical processes [5,6] the broad band with large intensity between 5 eV and 7 eV, typical for ethylene and its derivatives, has been investigated carefully. Most previous works assigned it to the $\pi\rightarrow\pi^*$ transition only, without any further analysis. Fig. 7a displays our measurements in this energy range over an expanded energy scale [11,12]. The corresponding Δ-plot is shown in Fig. 7b.

For the three isomers quantum chemical calculations have been performed [7–12]. Table 7 lists the energy position and the rough main character of the valence and Rydberg states involved in these transitions. In many cases vibrational progressions are observed [11,12]. Clearly, the band position sequence follows the trend cis>1,1>trans. However, from Table 7, the location of the $\pi\rightarrow\pi^*$ transition energy is almost constant within experimental error. The lowest Rydberg $\pi\rightarrow$R3s transition energy decreases in the sequence 1,1>cis>trans following the trend of the corresponding first IE_{ad}. In most cases the $\pi\rightarrow\sigma^*$ transition involves an excited state of mixed valence/Rydberg nature.

Declaration of Competing Interest

The authors declare that they have no known competing financial interests or personal relationships that could have appeared to influence the work reported in this paper.

CRediT authorship contribution statement

R. Locht: Conceptualization, Funding acquisition, Data curation. **D. Dehareng:** Software. **B. Leyh:** Validation.

Acknowledgments

R.L. and B.L. are grateful to the European Community for its financial support through the TMR (Contract EU-HPRI-1999CT-00028) and I3 (Contract R II 3 CT-2004-506008) programs. D.D.'s contribution was supported by the Belgian program on Interuniversity Attraction Poles of the Belgian Science Policy(IAP n° P6/19).

Supplementary materials

Supplementary material associated with this article can be found, in the online version, at doi:10.1016/j.jqsrt.2020.107048.

References

[1] Mahncke HE, Noyes WA Jr. J Chem Phys 1935;3:536.
[2] Walsh AD. Trans Faraday Soc 1945;41:35.
[3] Goto K. Sci Light 1960;9:104.
[4] Walsh AD, Warsop PA. Trans Faraday Soc 1968;64:1418.
[5] Berry MJ. J Chem Phys 1974;61:3114.
[6] Seki K, Kobayashi T, Ebata K. J Photochem 2011;219:200.
[7] Khvostenko OG. J Electr Spectr Rel Phenom 2014;195:220.
[8] Koerting CF, Walzl KN, Kuppermann A. Chem Phys Lett 1984;109:140.
[9] Williams BA, Cool AA. J Phys Chem 1993;97:1270.
[10] Arulmozhiraja S, Ehara M, Nakatsuji H. J Chem Phys 2008;129:174506.
[11] Locht R, Dehareng D, Leyh B. J Phys Commun 2017;1:045013; J Phys Commun 2017;1:055030.
[12] Locht R, Dehareng D, Leyh B. AIP Adv 2019;9:015305.
[13] R. Locht, D. Dehareng, B. Leyh, unpublished results.
[14] Hoxha A, Locht R, Leyh B, Dehareng D, Jochims H-W, Baumgärtel H. Chem Phys 2000;256:239; Locht R, Dehareng D, Leyh B. Mol Phys 2014;112:1520.
[15] Locht R, Leyh B, Hoxha A, Dehareng D, Jochims H-W, Baumgârtel H. Chem Phys 2000;257:283.
[16] Locht R, Dehareng D, Leyh B. J Phys B 2014;47:085101.
[17] Palmer MH, Ridley T, Hoffmann SV, Jones NC, Coreno M, de Simone M, Grazioli C, Zhang T, Biczysko M, Baiardi A, Peterson KA. J Chem Phys 2016;144:204305; J Chem Phys 2016;144:124302; ibid. 2015. J Chem Phys 2015;143:164303.
[18] Marmet P. Rev Sci Instrum 1979;50:79; Carbonneau R, Bolduc E, Marmet P. Can J Phys 1973;51:505; Carbonneau R, Marmet P. Can J Phys 1973;51:2203; ibid. Phys Rev 1974;A 9:1898.
[19] Mohr PJ, Taylor BN, Newell DB. J Phys Chem Ref Data 2016;45:043102; Mohr PJ, Newell DB, Taylor BN. Rev Mod Phys 2016;88:035009.
[20] Frisch MJ, Trucks GW, Schlegel HB, Scuseria GE, Robb MA, Cheeseman JR, Scalmani G, Barone V, Mennucci B, Petersson GA, Nakatsuji H, Caricato M, Li X, Hratchian HP, Izmaylov AF, Bloino J, Zheng G, Sonnenberg JL, Hada M, Ehara M, Toyota K, Fukuda R, Hasegawa J, Ishida M, Nakajima T, Honda Y, Kitao O, Nakai H, Vreven T, Montgomery JA Jr, Peralta JE, Ogliaro F, Bearpark M, Heyd JJ, Brothers E, Kudin KN, Staroverov VN, Kobayashi R, Normand J, Raghavachari K, Rendell A, Burant JC, Iyengar SS, Tomasi J, Cossi M, Rega N, Millam JM, Klene M, Knox JE, Cross JB, Bakken V, Adamo C, Jaramillo J, Gomperts R, Stratmann RE, Yazyev O, Austin AJ, Cammi R, Pomelli C, Ochterski JW, Martin RL, Morokuma K, Zakrzewski VG, Voth GA, Salvador P, Dannenberg JJ, Dapprich S, Daniels AD, Farkas O, Foresman JB, Ortiz JV, Cioslowski J, Fox DJ. Gaussian 09, Revision A.*02*. Wallingford CT: Gaussian Inc.; 2009.
[21] Dunning TH Jr. J Chem Phys 1989;90:1007.
[22] Cizek J. Adv Chem Phys 1969;14:35.
[23] Scuzeria GE, Schaefer HF III. J Chem Phys 1989;90:3700.
[24] Zhao Y, Truhlar DG. Theor Chem Acc 2008;120:215.
[25] Van Caillie C, Amos RD C. Chem Phys Lett 2000;317:159.
[26] Von Niessen W, Åsbrink L, Bieri G. J Electr Spectry Rel Phenom 1982;26:173.
[27] Parkes MA, Ali S, Howle CR, Tuckett RP, Malins AER. Mol Phys 2007;105:907.
[28] Berndtsson A, Basilier E, Gelius U, Hedman J, Klasson M, Nilsson R, Nordling C, Svensson S. Phys Scripta 1975;12:235.

[29] Mei L, Chuaqui M, Mathers CP, Ying JF, Leung KT. Chem Phys 1994;188:347.
[30] Takeshita K. J Chem Phys 1999;110:6792.
[31] Woo HK, Wang P, Lau KC, Xing X, Ng CY. J.Chem.Phys. 2004;108:9637.
[32] Bae YJ, Lee M, Kim MS. J Phys Chem A 2006;110:8535.
[33] Shimanouchi T. Tables of Vibrational Frequencies, Consolidated Vol.1.. NSRD-S-NBS; 1972. p. 39.
[34] Herzberg G. Molecular spectra and molecular structure. *III. Electronic spectra and electronic structure of polyatomic molecules*. New Jersey: D. Van Nostrand Company Inc. Princeton; 1967. p. 132.
[35] Locht R, Leyh B, Dehareng D, Jochims H-W, Baumgärtel H. Chem Phys 2009;362:97; Locht R, Jochims HW, Leyh B. Chem Phys 2012;405:124; Locht R, Dehareng D, Leyh B. Mol Phys 2014;112:1520.